

Fast microfocus x-ray tube based on carbon nanotube array

Xiaobing Li, Juntao Zhou, Qingyang Wu, Menglong Liu, Rifeng Zhou, and Zexiang Chen

Citation: *Journal of Vacuum Science & Technology B* **37**, 051203 (2019); doi: 10.1116/1.5099697

View online: <https://doi.org/10.1116/1.5099697>

View Table of Contents: <https://avs.scitation.org/toc/jvb/37/5>

Published by the [American Vacuum Society](#)

HIDEN
ANALYTICAL

Instruments for Advanced Science

Contact Hiden Analytical for further details:

W www.HidenAnalytical.com
E info@hiden.co.uk

CLICK TO VIEW our product catalogue



Gas Analysis

- ▶ dynamic measurement of reaction gas streams
- ▶ catalysis and thermal analysis
- ▶ molecular beam studies
- ▶ dissolved species probes
- ▶ fermentation, environmental and ecological studies



Surface Science

- ▶ UHV TPD
- ▶ SIMS
- ▶ end point detection in ion beam etch
- ▶ elemental imaging - surface mapping



Plasma Diagnostics

- ▶ plasma source characterization
- ▶ etch and deposition process reaction kinetic studies
- ▶ analysis of neutral and radical species



Vacuum Analysis

- ▶ partial pressure measurement and control of process gases
- ▶ reactive sputter process control
- ▶ vacuum diagnostics
- ▶ vacuum coating process monitoring



Fast microfocus x-ray tube based on carbon nanotube array

Xiaobing Li,^{1,a)} Juntao Zhou,^{1,a)} Qingyang Wu,² Menglong Liu,¹ Rifeng Zhou,³ and Zexiang Chen^{1,2,b)}

¹School of Optoelectronic Science and Engineering, University of Electronic Science and Technology of China, 610054 Chengdu, China

²Guangzhou Haozhi Imaging Technology Co. Ltd, 400044 Guangzhou, China

³Industrial CT Center, Chongqing University, 400044 Chongqing, China

(Received 12 April 2019; accepted 17 July 2019; published 16 August 2019)

A full vacuum-sealed macrofocus x-ray tube with a vertically-aligned ring-shaped carbon nanotube (CNT) emitter grown by microwave plasma enhanced chemical vapor deposition is presented in this paper. The external grid allowed the CNT-based x-ray tube to exhibit transient switching on and off. The total emission current was 200 μ A, which corresponds to a maximum emission current density of 10.1 A/cm² from the ring-shaped CNT emitter when the grid voltage was 2.4 kV. The optimized focus electrode controlled the beam convergence on the target to produce a very small x-ray focal spot size less than 5 μ m. Consequently, this microfocus x-ray tube could produce x-ray images with very high spatial resolution. X-ray fluoroscopy images of a multilayer printed circuit board (PCB) and field programmable gate array show distinct gold PCB traces with approximately 20 μ m width. *Published by the AVS.* <https://doi.org/10.1116/1.5099697>

I. INTRODUCTION

Carbon nanotubes (CNTs) are a very attractive field emitter for vacuum electronic devices due to their high aspect ratio, high electric conductivity, and high mechanical, chemical, and thermal stability.¹⁻⁵ Field emission with more than 2 A/cm² current density from CNT emitters has been reported.⁶⁻¹¹ The development of CNT-based electron field emitters has prompted the creation of a new class of electronic vacuum devices, such as field emission displays, microwave amplifiers, and x-ray tubes.¹²⁻¹⁷

CNT field emission x-ray tubes provide fast switching, digital addressing, and rapid snapping with potential applications in a number of fields. A prototype of CNT-based x-ray tube and CT system with a CNT x-ray source was developed by Zhou's group.¹⁸⁻²¹ Cho reported a miniaturized x-ray tube with small, flat-tipped CNT emitters with the diameter of 0.8 mm.²² Fully vacuum-sealed CNT-emitter x-ray tubes without an active pump were reported by several research groups,²¹⁻²⁹ in which diode or triode structures were configured and focusing lenses were used to produce a small focal spot in some cases. Conventional thermal-cathode x-ray tubes cannot act as monochromatic x-ray sources, but field emission technology could provide monochromatic x-rays. A direct quasimonochromatic x-ray source based on CNT emitter was developed successfully by favoring the L-peak emission over the Bremsstrahlung part.³⁰

Generally, a CNT emitter plays a key role in those x-ray tubes mentioned above. There are two typical methods for fabricating a CNT emitter. The first is a two-step method, where CNTs are initially grown and then mounted on a substrate by screen printing²¹⁻²⁴ or electrophoresis.^{8,31} This is an economic and efficient method, but it is difficult to vertically

align and evenly distribute the CNTs while wiping off the residual product from the paste. The second is a direct synthesis method, where CNTs are grown on a substrate to form an emitter using various chemical vapor deposition (CVD) methods.⁶⁻⁹ However, the natural limitations on their operational characteristics, which arise due to electric field screening effects in CNT arrays, thermal effects, and statistical spread in parameters of individual nanotubes, have become critical issues that hinder their application in power devices, where CNTs must emit a large stable current. The CNT emission current density in these devices was low and should be improved.

Here, we report a CNT-based x-ray tube with small focal spot, in which a ring-shaped CNT emitter was grown by microwave plasma CVD, yielding a field emission cathode with stable emission current. An electron gun with a grid gate and a focus electrode were designed for this x-ray tube to provide a micrometer level x-ray focal spot. The full vacuum-sealed microfocus CNT-based x-ray tube exhibited reliable digital operation at high emission current density with fast switching.

II. EXPERIMENT

A. CNT fabrication

In order to produce a smaller symmetric electron beam focus and sufficiently large field emission current, the cathode pattern was designed as a cylindrical array pattern with a maximum diameter of 50 μ m according to our simulations, as shown in Fig. 1. There are three circles in this pattern. The largest circle was 50 μ m in diameter, the next smaller ring was 20 μ m in diameter, and the thickness of the circles was 2 μ m. The diameter of the central circle was 5 μ m.

A standard lithographic method was used to pattern catalyst layers for CNT growth on a silicon wafer. CNT arrays with high current density, stable current, and high adhesion

^{a)}X. Li and J. Zhou contributed equally to this work.

^{b)}Author to whom correspondence should be addressed: zxchen@uestc.edu.cn

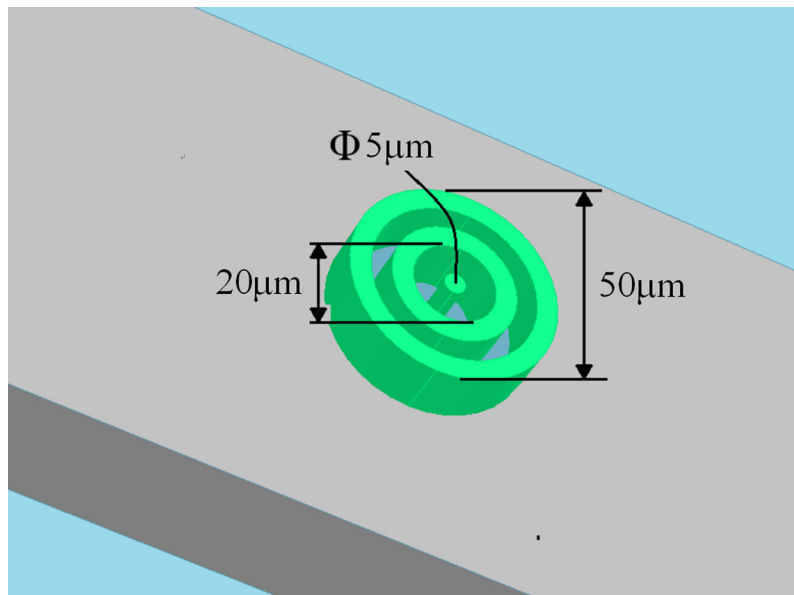


FIG. 1. Model of the carbon nanotube emitter.

strength to the substrate were obtained by designing a unique stacked multilayer metal structure to grow CNTs. These CNTs will have larger current density. First, a thick layer of TiN (200 nm) was deposited on a silicon substrate by sputtering and was subsequently covered with a photoresist pattern. Next, copper and aluminum layers with 100 and 5 nm thickness, respectively, were deposited through evaporation as a buffer layer. The TiN and copper layers both increase the adhesion strength of the CNTs and increase the electrical and thermal conductivities. The aluminum layer has a dispersing and limiting effect on the iron particles such that the iron catalyst particles can be dispersed uniformly without significant agglomeration, which prevents the CNT density from becoming too large in a partial region.⁸ Finally, a layer of iron (2.5 nm) was evaporated to act as a source for the catalyst particles. The catalyst pattern was obtained after stripping the photoresist layer.

CNT growth was performed in a microwave plasma CVD reactor operating at 2.45 GHz.³² CNTs were grown at

1 kW microwave power, 25 mbar internal reactor pressure, and 200 sccm gas flow rate with a $\text{CH}_4 + \text{H}_2$ mixture at a 9:1 ratio. A radio frequency heater was used to preheat the sample to the deposition temperature of approximately 650 °C, and the hydrogen plasma was ignited with an additional energy source. After keeping the sample at a constant temperature of 650 °C for 5 min, the thin Fe-layer was converted into nanoparticles and then methane was injected into the hydrogen plasma to induce CNT growth for 1–3 min.

B. X-ray tube fabrication

The electrodes were optimized based on a series of the electron optics simulation conducted with OPERA 3D software. Figure 2 shows the electron gun simulation structure.

A grid with a 200 μm diameter round hole with 0.1 mm thickness was used as a gate to extract electrons from the CNT cathode. The distance between the CNT emitter and

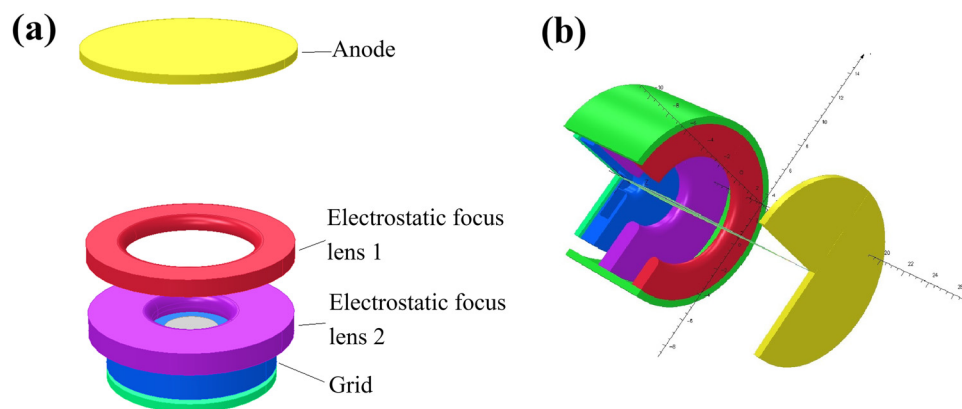


FIG. 2. Electron gun simulation structure. (a) Schematic model of the microfocus x-ray tube based on CNT array using OPERA 3D simulation software. (b) Final optimized electron gun simulation structure.

TABLE I. Effects of the manipulated variables on the FSS. Each set of data surrounded by gray boxes represents a situation in which a parameter changes in a trend. The last row of data represents the optimal parameters.

Condition	Voltage of grid (mm)	Position of focus lens 1 (mm)	Inner diameter of focus lens 1 (mm)	Position of focus lens 2 (mm)	Inner diameter of focus lens 2 (mm)	FSS (μm)
1	1	4	5	7	7	48
	2	4	5	7	7	34
	3	4	5	7	7	26
	4	4	5	7	7	15
	5	4	5	7	7	9
2	3	2	5	7	7	21
	3	3	5	7	7	23
	3	4	5	7	7	26
	3	5	5	7	7	35
	3	6	5	7	7	25
3	3	4	3	7	7	71
	3	4	4	7	7	26
	3	4	5	7	7	6
	3	4	6	7	7	15
	3	4	7	7	7	25
4	3	4	5	5	7	8
	3	4	5	6	7	15
	3	4	5	7	7	26
	3	4	5	8	7	33
	3	4	5	9	7	31
5	3	4	5	7	5	67
	3	4	5	7	6	43
	3	4	5	7	7	26
	3	4	5	7	8	16
	3	4	5	7	9	31
6	3	4	5	7	8	5

grid was about $250\mu\text{m}$. The focusing electrode is an essential component in a field emission electron gun. It plays a key role in converging the electron beam to a small spot on the anode. We designed a focusing electrode with two focusing rings with different diameters. In our design, the focus voltage ranged from 0 to 500 V to produce fine convergence. The simulated focal spot size on the target was less than $5\mu\text{m}$ when the anode voltage was 80 kV.

Table I shows the effects of the manipulated variables on the focus spot size (FSS) of the electron beam. Five different parameters, in turn, were simulated and optimized to get focus spot size.

1. Effect of the applied voltage at the grid

The voltage range of the grid from 1 to 5 kV was applied to investigate the influence to the electron beam. The simulation results show that the FSS decreased as the voltage at the gate increased.

2. Effect of the axial distance of the first electrostatic lens

In our simulation results, the beam radius increased when the axial distance increased from 2 to 5 mm away from the cathode. However, the FSS started to decrease after the axial distance is more than 5 mm because the lens moved nearer the second focus lens.

3. Effect of the geometrical inner diameter of the first focus lens

The geometrical inner diameter of the first focal lens was changed from 3 to 7 mm. As the inner diameter of the lens increased from 3 to 5 mm, the FSS decreased. However, the FSS increased when the inner diameter continues to increase from 5 to 7 mm.

4. Effect of the axial distance of the second electrostatic lens

The axial distance of the second electrostatic lens was varied from 5 to 9 mm with respect to the cathode assembly. It was observed that as the distance of the anode increased from the cathode assembly, the FSS also increased. Beyond 8 mm, the FSS started to decrease.

5. Effect of the geometrical inner diameter of the second focus lens

As the inner diameter of the lens increased from 5 to 8 mm, the FSS decreased from 67 to $16\mu\text{m}$. However, when the inner diameter continues to increase from 8 to 9 mm, the radius of the beam increases from 16 to $31\mu\text{m}$.

Eventually, we obtained an optimized FSS value based on the results obtained above. The simulation structure parameters with the FSS of $5\mu\text{m}$ were obtained. Figure 3 shows the simulation results for the optimized electron gun.

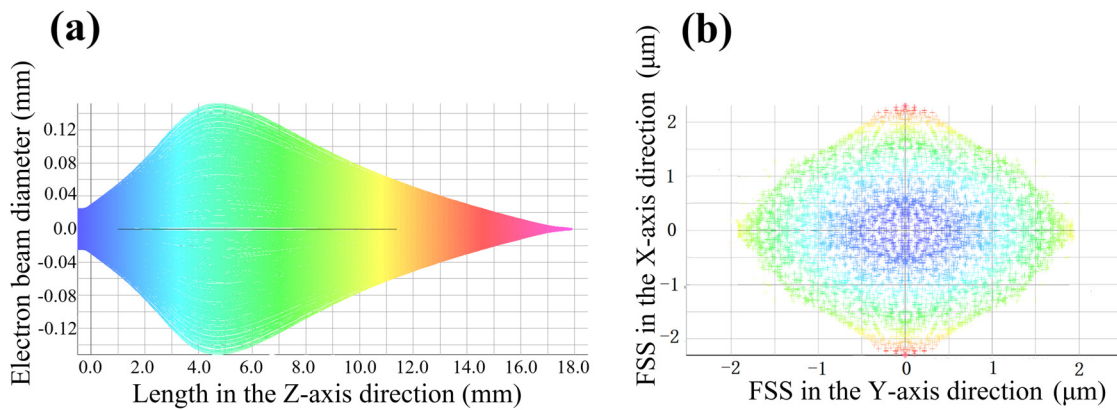


FIG. 3. Simulation results. (a) Electron beam trajectories, (b) FSS of the cross section on the target.

Based on the simulation results, an electrostatic gun was designed for this microfocus x-ray tube. A cylinder copper anode with a takeoff angle of 14° was used as a target. This causes x-rays emitted along the vertical direction to be compressed, and the width of the x-ray beam will be thinner. A tungsten plate was welded on the anode surface where electrons bombard with high energy.

The electron gun and anode were housed in a glass tube to form an unsealed x-ray tube. The unsealed tube was pumped down to 5×10^{-6} Pa with a mechanical pump and a turbo molecular pump, subsequently followed by baking at 550°C for 12 h. An evaporable getter was mounted beneath the CNT cathode to ensure that the vacuum in the x-ray tube remained high in order to guarantee stable operation at 80 kV.

C. Measurement of field emission

Figure 4 shows a schematic of the direct radiography testing system. A high voltage generator with voltage ranging from 0 to 90 kV was applied to the anode of the x-ray tube, and the cathode was set to zero potential. In order to achieve better focusing in the x-ray tube, the focusing electrode was connected

to a voltage source that could be accurately controlled from 0 to 500 V. The gate of the x-ray tube, which was connected to an adjustable high voltage DC power supply, provided a strong electric field to the tip of CNTs to extract electrons from the CNTs. The x-ray detector received penetrated x-rays to form an image signal, which was then transferred to a computer.

Field emission measurements of CNT arrays were gathered. First, we tested the field emission current of the x-ray tube. At this time, the anode voltage was set as the working voltage and remained unchanged. When the grid voltage gradually increased, the field emission from the CNT cathode began once a threshold was reached. The total current could be measured by sampling the voltage drop across a resistor.

III. RESULTS AND DISCUSSION

A high-resolution field emission scanning electron microscope (FE-SEM, Inspect FEI) was used to examine the as-grown CNT electron emission source. SEM images of the as-grown CNT array are shown in Fig. 5.

SEM images of the as-grown CNT array show that the CNT-bundles have a length of about $15\ \mu\text{m}$ with $10\ \mu\text{m}$

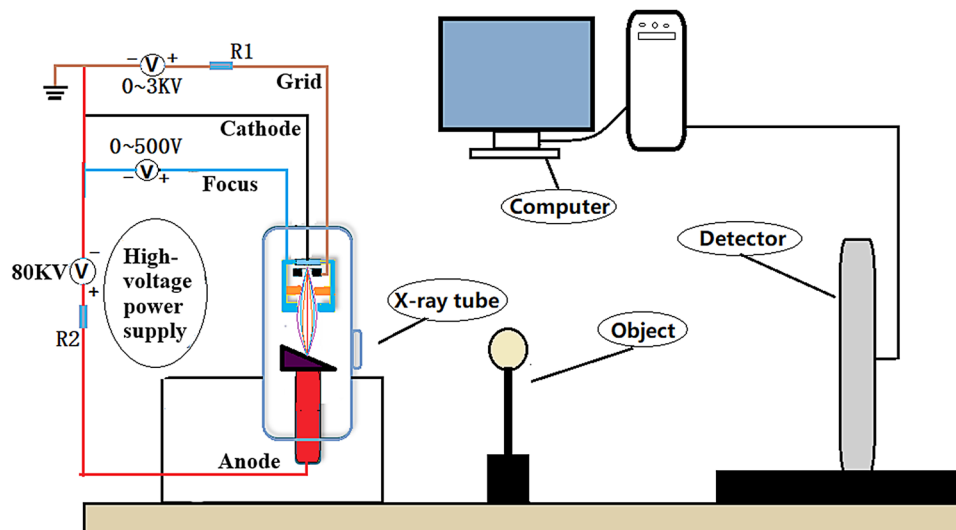


FIG. 4. Digital radiography system schematic.

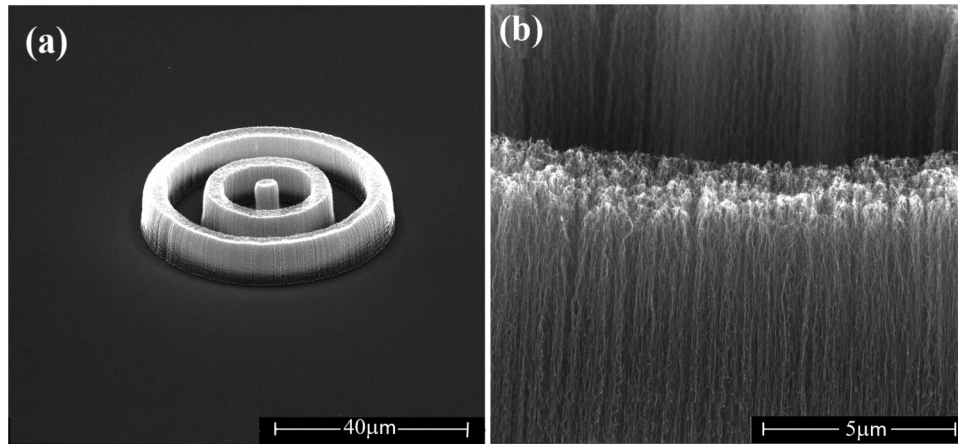


FIG. 5. SEM image of an as-grown CNT array. (a) Overall shape of the CNT array. (b) Higher resolution image of the CNT array.

pitch. All CNT-bundles were oriented vertically on the substrate and formed an excellent emitter pattern throughout the sample. Uniformity in the height of CNTs plays an important role in providing a stable field emission current, where every CNT contributes to the field emission current. The sample can provide a homogenous emission current from every emitter at any electric field, preventing the formation of hot spots and burning of individual CNTs that stick out from the cathode plane. Beside, Strong adhesion between carbon tube and substrate can be produced as a result of unique stacked multilayer metal structure.

The current from the fully vacuum-sealed x-ray tube was measured. Figure 6 shows the prepared x-ray tube, and the diameter and the overall length of the tube are 30 and 70 mm, respectively. The I-V curve is shown in Fig. 7. A total emission current of $200\ \mu\text{A}$ was obtained at 2.4 kV gate voltage. The corresponding emission current density could reach more than $10.1\ \text{A}/\text{cm}^2$. At present, the current density emitted from most CNT field emission cathodes is below $5\ \text{A}/\text{cm}^2$. The threshold field, corresponding to an emission current density of $10\ \text{mA}/\text{cm}^2$, is about $4\ \text{V}/\mu\text{m}$, which is also higher than that reported by others.^{5,8,19}

The reason why the threshold field is higher could be due to the electric field shielding because the CNT bundle is very short. Simulations show that the emitter could exhibit optimized performance when the distance between rings in the array is equal to the height of the CNTs, as this balances field screening effects.²⁰

The resolution test pattern based focal spot measurement technique has been widely used. We used a line test pattern to make a preliminary assessment of the spatial resolution of the CNT-base x-ray tube. The resolution test pattern consisted of seven segments ranging from 2.5 to 20 line pairs per mm. Figure 8 shows the experimental measurement of the spatial resolution. As can be seen from Fig. 8, the image is still very sharp when the line density is 20 pairs per millimeter. It can be judged that its true resolution is better than 20 lp/mm.

Finally, we analyzed some images gathered with our x-ray tube. Images of a multilayer memory module were gathered at approximately $6\times$ magnification to gather images of the inner structure of the printed circuit board (PCB). The pixel size of the detector was $75\times 75\ \mu\text{m}^2$, as shown in Fig. 9. Traces on the inner layers of the PCB can be seen in

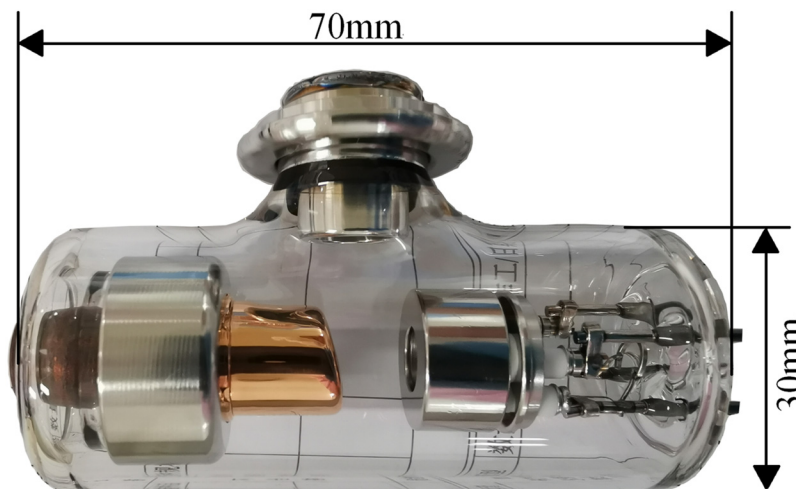


FIG. 6. Picture of the fully sealed x-ray tube.

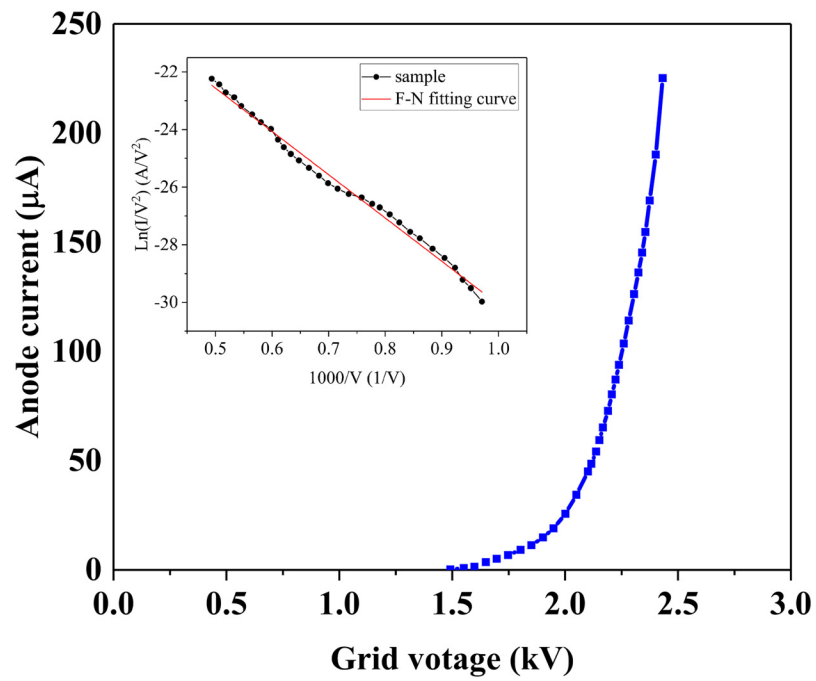


FIG. 7. Field emission I-V test curve. The anode voltage was set to 80 kV and the gate voltage was adjusted from 1 to 2.5 kV.

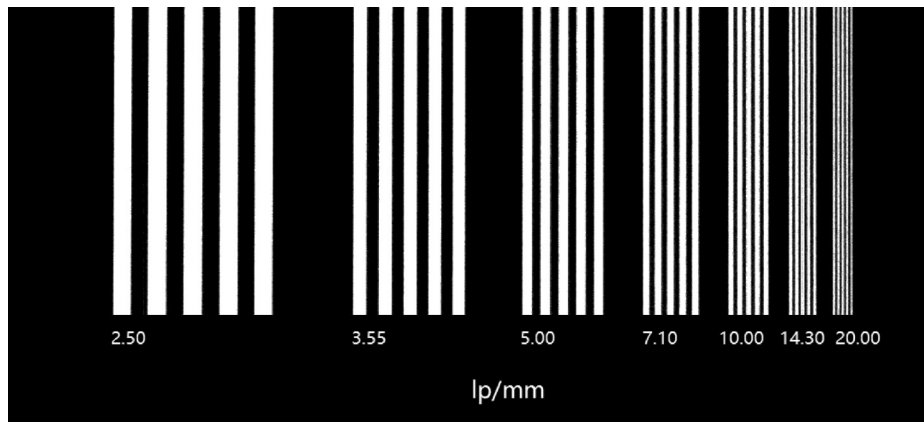


FIG. 8. Experimental measurement of the spatial resolution.

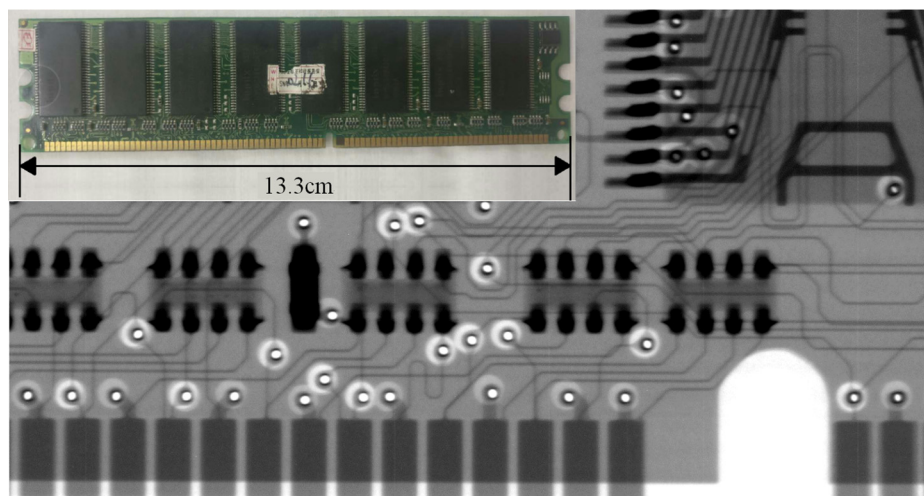


FIG. 9. X-ray image of a memory module on a PCB.

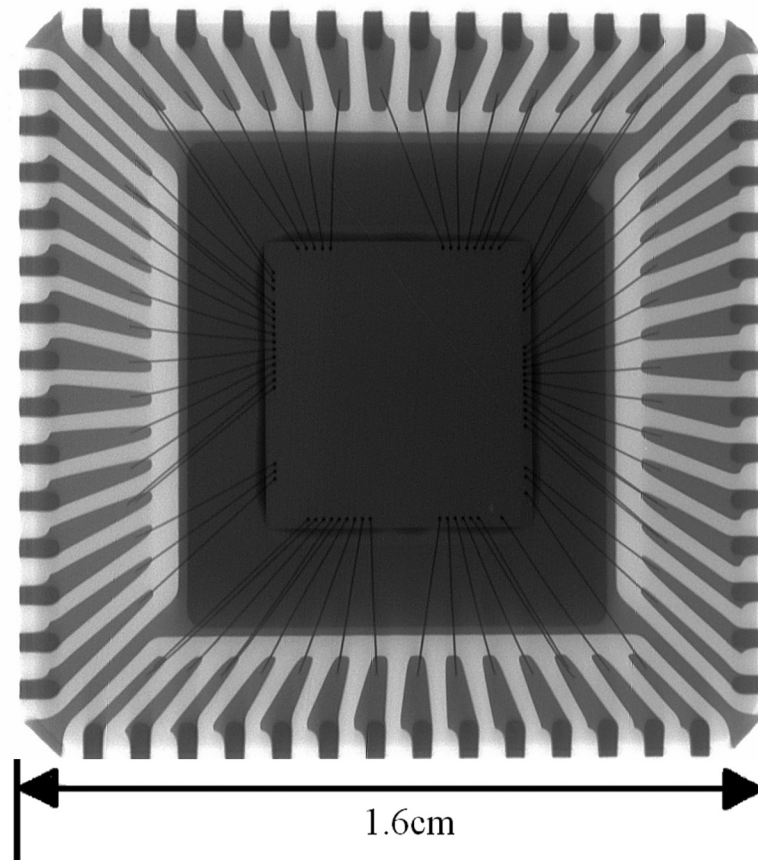


FIG. 10. X-ray image of an FPGA.

the x-ray image, indicating that the x-ray focal spot size of the CNT-ray tube is very small.

Figure 10 shows the distribution of leads inside a 1 mm thick FPGA. The image in this figure was gathered at 80 kV and is magnified by a factor 10 to allow the very thin electrical leads to be seen clearly. The finest gold wire in the chip was approximately $20\ \mu\text{m}$ wide, and its position can be seen clearly. As the results show, the small x-ray focal spot size could produce x-ray images with high spatial resolution.

IV. CONCLUSIONS

Fine-patterned CNT arrays for field emission were fabricated by microwave plasma enhanced chemical vapor deposition. These CNT arrays produced very high emission current density of $10.1\ \text{A}/\text{cm}^2$. An electron gun with two ring-shaped focusing electrodes was optimized to produce fine electron beam convergence. Finally, a fully sealed x-ray tube was fabricated and tested. Anode operating current can reach $200\ \mu\text{A}$. Also, we analyzed x-ray projection images to determine the actual resolution of the x-ray tube. The x-ray tube can produce x-rays with resolutions higher than $20\ \text{lp}/\text{mm}$. The finest gold wire with a diameter of $20\ \mu\text{m}$ in the FPGA chip can be clearly distinguished. Whether it is the working current of the tube or the resolution, it has reached the leading level in the field of microfocus x-ray tubes.

ACKNOWLEDGMENTS

The authors are grateful for financial support from the National Natural Science Foundation of China (NSFC) (Nos. 61071027 and 51702037) and the Fundamental Research Funds for the Central Universities of China (No. ZYGX2015KYQD014).

- ¹S. T. Purcell, P. Vincent, C. Journet, and V. T. Binh, *Phys. Rev. Lett.* **88**, 105502 (2002).
- ²N. de Jonge, Y. Lamy, K. Schoots, and T. H. Oosterkamp, *Nature* **420**, 393 (2002).
- ³A. V. Eletsii, *Phys. Usp.* **53**, 863 (2010).
- ⁴J.-H. Lee, S. H. Lee, D. Kim, and Y. S. Park, *Thin Solid Films* **546**, 94 (2013).
- ⁵G. Chen, D. N. Futaba, S. Sakurai, M. Yumura, and K. Hata, *Carbon* **67**, 318 (2014).
- ⁶E. Minoux *et al.*, *Nano Lett.* **5**, 2135 (2005).
- ⁷S. Fujii, S.-I. Honda, H. Machida, H. Kawai, K. Ishida, M. Katayama, H. Furuta, T. Hirao, and K. Oura, *Appl. Phys. Lett.* **90**, 153108 (2007).
- ⁸J. L. Silan, D. L. Niemann, B. P. Ribaya, M. Rahman, M. Meyyappan, and C. V. Nguyen, *Solid State Electron.* **54**, 1543 (2010).
- ⁹C. Li *et al.*, *Appl. Phys. Lett.* **97**, 113107 (2010).
- ¹⁰E. Rahman and A. Nojeh, *Nanotechnology* **30**, 175202 (2019).
- ¹¹W. Zhu *et al.*, *Nanotechnology* **28**, 305704 (2017).
- ¹²K. B. K. Teo *et al.*, *Nature* **437**, 968 (2005).
- ¹³A. A. Kuznetsov, S. B. Lee, M. Zhang, R. H. Baughman, and A. A. Zakhidov, *Carbon* **48**, 41 (2010).
- ¹⁴Y. Z. Lee, L. Burk, K. H. Wang, G. Cao, J. Lu, and O. Zhou, *Nucl. Instrum. Meth. A* **648**, S281 (2011).
- ¹⁵D. Li, Y. Cheng, M. Cai, J. Yao, and P. Chang, *Sci. China Phys. Mech.* **56**, 2081 (2013).

- ¹⁶D. Li, Y. Wang, Y. Cheng, Y. Feng, L. Zhao, H. Zhang, J. Sun, and C. Dong, *J. Phys. D Appl. Phys.* **48**, 47 (2015).
- ¹⁷A. Sharma, H. S. Kim, D.-W. Kim, and S. Ahn, *Microelectron. Eng.* **152**, 35 (2016).
- ¹⁸Y. Cheng and O. Zhou, *C. R. Phys.* **4**, 1021 (2003).
- ¹⁹N. J. Pelc, J. Shan, O. Zhou, J. Lu, R. M. Nishikawa, and B. R. Whiting, "Anode thermal analysis of high power microfocus CNT x-ray tubes for in vivo small animal imaging," in *Medical Imaging 2012: Physics of Medical Imaging*, edited by N. J. Pelc, R. M. Nishikawa and B. R. Whiting (2 March 2012).
- ²⁰X. Qian *et al.*, *Med. Phys.* **39**, 2090 (2012).
- ²¹E. Gidcumb, B. Gao, J. Shan, C. Inscoc, J. Lu, and O. Zhou, *Nanotechnology* **25**, 245704 (2014).
- ²²H. J. Kim, J. M. Ha, S. H. Heo, and S. O. Cho, *J. Nanomater.* **2012**, 854602 (2012).
- ²³G. Chen, B. Zhao, H. Kimura, H. Kurachi, N. Matsumoto, T. Yamada, K. Hata, S. Uemura, and D. N. Futaba, *Mater. Res. Express.* **4**, 105041 (2017).
- ²⁴J. W. Jeong, J. W. Kim, J. T. Kang, S. Choi, S. Ahn, and Y. H. Song, *Nanotechnology* **24**, 085201 (2013).
- ²⁵V. J. Scott, H. Manohara, R. Toda, L. Del Castillo, R. Murthy, J. Mulder, E. Murty, and M. C. Thompson, *Nanotechnology* **27**, 494002 (2016).
- ²⁶P. Liu *et al.*, *Nanotechnology* **29**, 345601 (2018).
- ²⁷J. H. Hong, J. S. Kang, and K. C. Park, *J. Vac. Sci. Technol. B* **36**, 02C109 (2018).
- ²⁸Y. Sun, D. A. Jaffray, and J. T. W. Yeow, *IEEE Trans. Electron Devices* **60**, 464 (2013).
- ²⁹A. A. Trubitsyn, E. Y. Grachev, and E. A. Kozlov, *J. Phys. Conf. Ser.* **1164**, 012022 (2019).
- ³⁰B. Diop and V. T. Binh, *Rev. Sci. Instrum.* **83**, 094704 (2012).
- ³¹F. Sprenger *et al.*, *Proc. SPIE Int. Soc. Opt. Eng.* **7622**, 76225M (2010).
- ³²Z. Chen, Q. Zhang, P. Lan, B. Zhu, T. Yu, G. Cao, and D. Engelsen, *Nanotechnology* **18**, 265702 (2007).